International Journal of Mass Spectrometry 280 (2009) 136–143

Contents lists available at ScienceDirect

International Journal of Mass Spectrometry

journal homepage: www.elsevier.com/locate/ijms

Surface neutralization/surface reionization (Ping–Pong) mass spectrometry

Changtong Hao [1], Luke E. Adams, Xinli Yang, Martin Sadílek, František Tureček *

Department of Chemistry, Bagley Hall, Box 351700, University of Washington, Seattle, WA 98195-1700, United States

ARTICLE INFO

Article history:
Received 6 June 2008
Received in revised form 9 July 2008
Accepted 18 July 2008
Available online 30 July 2008

This paper is dedicated to Zdenek Herman on the occasion of his 75th birthday and in appreciation of his many contributions to gas-phase ion chemistry.

Keywords:
Surface neutralization
Surface ionization
Instrument design
Pyridine
Benzene

ABSTRACT

Experiments are reported that utilize surface neutralization of hyperthermal organic ions to obtain hyperthermal neutral species that are reionized on oxygen-activated rhenium surface and detected by mass spectrometry. A special Ping–Pong mass spectrometer was designed and coupled to a double-focusing mass spectrometer to allow energy and angle-resolved measurements. Neutralization of pyridine and benzene ions on gold, copper, and aluminum surfaces generated substantial ion currents into the collecting plate. The ion currents obtained on gold surfaces were found to depend on the recombination energy of the ion projectile. Hyperthermal neutrals coming off the first surface were found to mainly originate from hydrocarbon adsorbates.

1. Introduction

Electron-based methods of ion dissociation have gained importance for mass spectrometric analysis of a range of organic and biologically important compounds. In an early approach introduced by Porter and Williams [1], gas-phase ions were discharged by collisional electron transfer from metal atoms at keV collision energies and the neutral intermediates were detected by a position-sensitive detector. This neutralized-beam method was later combined with another method using collisional reionization of neutral fragments [2] into neutralization–reionization mass spectrometry (NRMS) [3]. NRMS has been very successful in providing access to a large number of transient neutral intermediates, which were otherwise inaccessible by classical chemical or photochemical methods [4]. Various NRMS techniques have been developed [5], such as variable-time NRMS [6], neutral ion dissociation difference (NIDD)[7], neutral photoionization [8], and photodissociation [9] that provided information on neutral dissociation kinetics and the electronic states accessed by collisional electron transfer. Collisional electron transfer from gaseous alkali metal atoms is utilized in electron capture-induced dissociation (ECID) [10] of multiply protonated peptides which results in charge reduction or reversal followed by cation or anion detection.

There are several limitations of NRMS that prevent it from being widely applied in mass spectrometric analysis. A major limitation is the low efficiency of electron transfer in gas-phase collisions. Charge transfer at keV kinetic energies in collisions of gas-phase cations with neutral electron donors has cross-sections on the order of 10^{-15} cm^2 [4e,11], which are comparable to those for collisional excitation at the same kinetic energy. This results in ion to neutral conversions on the order of a few percent. Neutral reionization to cations is even less efficient (<1%), and thus the overall efficiency of the cation–neutral–cation process is typically <0.01% [12].

Another limitation is the need to carry out ion–atom or ion–molecule charge-transfer collisions at keV kinetic energies. This restricts the ion–electron donor interaction time to a few femtoseconds and often results in vibrational excitation in the neutral intermediate through Franck–Condon effects [13]. These can be particularly significant for even-electron cations and cause substantial dissociation of neutral intermediates formed by collisional electron transfer [14]. Franck–Condon factors also affect the formation of excited electronic states upon collisional electron transfer [15], whose analysis requires special techniques [9b] and the ensuing dissociations complicate NR mass spectra [16].

To circumvent the above-mentioned drawbacks of NRMS, we investigated the possibility of conducting the neutralizing and ionizing charge transfer collisions on surfaces. We call this method

* Corresponding author.
E-mail address: turecek@macmail.chem.washington.edu (F. Tureček).
[1] Present address: Department of Chemistry, York University, Toronto, Canada.

1387-3806/$ – see front matter © 2008 Elsevier B.V. All rights reserved.
doi:10.1016/j.ijms.2008.07.022

Ping–Pong NRMS, where Ping refers to the ion neutralizing collision on the first surface and Pong to the neutral-reionizing collision on the second surface. Here we present the instrument design and first results, and also discuss the merits and limitations of our approach.

Interactions of gas-phase ions with surfaces have been studied extensively for both atomic and polyatomic species [17]. In particular, ion neutralization upon collision with a surface has been an undesirable side-effect of surface-induced dissociation (SID) mass spectrometry that was introduced by Cooks and co-workers [18,19] and developed by Wysocki and co-workers [20], Hanley et al. [21], and others [22,23]. The yields of neutrals on untreated metal surfaces, as estimated from the loss of ion beam intensity, approach 90% for a number of atomic and organic cation-radicals and cations, indicating a very high conversion of ions to neutrals [24,25]. The interaction time for a hyperthermal ion colliding with surface atoms is estimated at ≈200 fs [26], which is substantially longer than the interaction time in gas-phase collisions of keV ions (2–10 fs). This may result in less severe Franck–Condon effects in ion-surface collisions. The kinetic energy of the scattered ions and neutrals shows strong angular dependence. Winters et al. have shown for Xe atoms that the fraction of the kinetic energy deposited in the surface followed a cos θ function where θ is the incidence angle with respect to the surface normal [27]. At >45 degrees >50% of the incident beam kinetic energy is retained in the scattered beam. In addition, Hanley et al. have shown for polyatomic ions that fragment ions scattered from surfaces had kinetic energy distributions similar to that of the undissociated ion [28]. These previous studies indicated that there was a range of kinetic energies, and incidence and final angles at which ions underwent efficient charge transfer neutralization with the surface, and the scattered neutrals retained a substantial fraction of the incident ion kinetic energy. All these factors appear to be favorable for the formation of hyperthermal neutrals to be studied by Ping–Pong NRMS.

Hyperthermal molecules striking a metal surface undergo ionization; the ion current can be approximated by the modified Saha–Langmuir equation (Eq. (1)) where γ is the fraction of the kinetic energy (E_k) used for ionization of the gas-phase molecule, A is a proportionality constant, ϕ is the metal work function,

$$I_{ion} = A\, e^{(\gamma E_k + \varphi - IE)/kT_s} \quad (1)$$

IE is the ionization energy of the gas-phase molecule, and T_s is the surface temperature [29]. Surface ionization of a variety of organic molecules has been reported by Fujii et al. [29–31] and Amirav et al. [32–34]. These authors reported that absolute ionization yields for amines on oxidized Pt(III) surfaces were in the low percent range at kinetic energies >4 eV, which is a ∼10 fold increase compared to gas-phase collisions, and which is promising for reionization of hyperthermal neutral species in Ping–Pong NRMS. Oxidized Pt ($\phi \approx 5.9$ eV) or Re ($\phi \approx 6.4$ eV) are the most common materials used for surface ionization [29,30], and the ionization efficiency can be boosted by using a hot surface at 800–1000 K. An attractive feature of surface ionization is that even molecules which are quite sensitive to thermal decomposition (e.g., cholesterol) can be ionized without causing excessive fragmentation [32].

Eq. (1) indicates that surface ionization yields mainly depend on the ionization energy and kinetic energy of the hyperthermal gas-phase molecules. This may favor detection of fragments, both radicals and molecules, having low ionization energies and masses close to that of the neutral precursor. For dissociations taking place in the gas-phase following the Ping collisions, the product kinetic energy is proportional to its mass, e.g., $T_{product} = T_{precursor}$ ($m_{product}/m_{precursor}$). In contrast, in dissociations occurring on the surface in the Ping collision, the products can be expected to have similar and nearly mass independent distributions of kinetic energies [28]. Due to the cos θ dependence on the incident Ping angle, selected dissociation products can be generated separately by scattering the corresponding ions at different angles, and the reionization efficiency in the Pong collision (Eq. (1)) can be calibrated at different kinetic energies. A potential drawback is that dissociation products having both high ionization energies and low masses (H_2O, NH_3, CO, N_2, etc) will be discriminated against. However, both Fujii [30,31] and Amirav [32,33] reported relatively efficient surface ionization on oxidized Re of aliphatic alcohols that had IE in the 10–10.5 eV range.

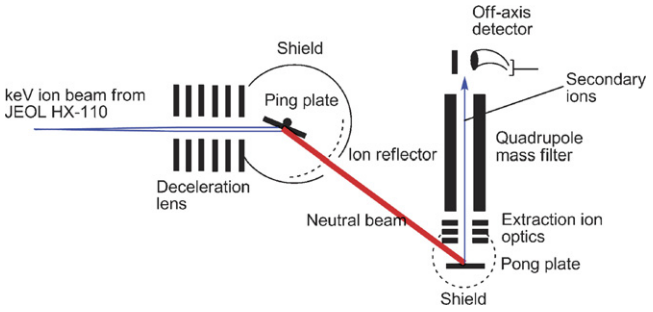

Fig. 1. Schematic diagram of the Ping–Pong NRMS instrument.

2. Experimental

The described experiments were performed on a home-built instrument consisting of a JEOL HX-110 double focusing sector mass spectrometer as MS-1 and a tandem surface collision chamber equipped with an Extrel quadrupole mass filter and Merlin data acquisition system as MS-2. The instrument design is described later in the pertinent sections. Ions were produced in an electron impact source at 70 eV electron energy, accelerated to 5 keV and mass selected. To pass mass-selected ions into the MS-2 chamber, the electron multiplier voltage was set to 0 V and the conversion dynode of the JEOL HX-110 instrument was grounded. Ions entering the MS-2 chamber were detected as total ion current using the Ping plate as an ion collector.

3. Results and discussion

3.1. Instrument design and overview

The new apparatus consists of a vacuum chamber containing a deceleration lens set, the Ping and Pong surfaces, extraction ion optics, and a MAXM5001 ABB Extrel quadrupole mass filter with an off-axis detector. A schematic layout is shown in Fig. 1. A large-scale JEOL HX-110 double-focusing mass spectrometer generates and mass-selects precursor ions. The JEOL mass spectrometer can be operated in the 1–10 keV range of ion kinetic energies. Ions of 5 keV kinetic energy were typically used for the Ping–Pong experiments. The mass resolution at full ion transmission of the JEOL instrument with all slits fully open is >1000. The ion beam exiting from the JEOL magnet sector is focused in the x–y horizontal plane at ∼0.6° divergence angle at the mass resolving γ slit. The z-axis height of the beam is less than 8 mm. The ion beam is decelerated to 5–100 eV by a special multi-element lens and refocused to a tight paraxial beam of less than 2 mm width. The 5–100 eV ion beam impinges on the Ping plate at a large incident angle to the surface normal. The optimum range of incidence angles is found experimentally. The Ping plate is floated at the deceleration potential and protected from the external fields by a cylindrical shield. The scattered neutrals are transmitted at a variable angle, while all residual ions are stopped by a 95% transmission metal mesh which is floated at ca. 50 V above the Ping plate potential. Neutral prod-

ucts pass the mesh and impinge on the Pong plate. The Pong plate is made of materials allowing surface ionization and mounted so that it could be resistively heated to 800–1200 K. Ions formed at the Pong plate are extracted by an electrostatic zoom lens and mass analyzed by the quadrupole mass filter with an off-axis detector. The beam incidence angle at the Ping plate (θ) can be adjusted step-wise by the rotation motion feedthrough. The angle for the neutrals scattered off the Ping plate (ψ) to strike the Pong plate is given by the following equation:

$$\psi = 180 - \left(\vartheta + \text{arctg}\frac{l}{d}\right) \quad 45^\circ \le \psi \le 90^\circ \tag{2}$$

where the angles refer to the Ping surface normal, d is the fixed distance from the center of the Ping plate to the quadrupole mass filter axis (10 cm), and l is the variable distance (0–10 cm) from the incident ion beam axis to the center of the Pong plate. Distance l is selected by translating the Pong plate along the quadrupole mass filter axis and refocusing the ion extractor lens potentials. The quadrupole mass filter is mounted in a fixed position. This appears to be a technically preferred solution for the first-generation instrument. One possible drawback is that the ions coming off the Pong plate have different flight times, depending on the plate distance from the mass filter.

3.2. Vacuum chamber and pumping system

Vacuum in the JEOL flight tube is maintained at ca. 1.3×10^{-6} Torr by one 3″ and two 4″ diffusion pumps, which are backed by 100 L/min roughing pumps. The Ping–Pong NRMS vacuum chamber is differentially pumped to a background pressure of 5.5×10^{-7} Torr by a 150 L/s turbomolecular pump (Alcatel ATP150), which is backed by a roughing pump (Edwards M8). The JEOL off-flange, located at the end of the dynode and electron multiplier assembly in the line of sight of the ion beam, was replaced by a KF50 flange to allow a gate valve (MDS KGV-1500V) to be mounted and connect the JEOL vacuum housing to the Ping–Pong NRMS vacuum chamber. The background pressure in the Ping–Pong chamber was 8×10^{-7} Torr when the gate valve was open.

The Ping–Pong NRMS vacuum chamber is fabricated from 3/8″ (9.52 mm) thick 304 stainless steel plates. The chamber has an internal floor area of 12.5×14 square inch and an internal height of 6 in. (Fig. 2). The chamber opens from the top with a removable lid. The top surface of the chamber walls is flat and polished for an O-ring seal. The lid is made of aluminum and has a O-ring groove milled into its underside to accommodate a 17″ long O-ring (Eriks West). The vacuum chamber sits atop four 1/4″ threaded rods; the nuts supporting the chamber can be adjusted to precisely level the vacuum chamber with the exit flange of the JEOL vacuum housing.

3.3. Ion deceleration lens

Ions exiting from the JEOL mass spectrometer must be decelerated from 5–10 keV to 5–100 eV kinetic energies for surface neutralization. This is achieved by an electrostatic lens system mounted directly behind the entrance to the Ping–Pong NRMS vacuum chamber. Simultaneously, the lens refocuses the ions into a paraxial beam before they collide with the Ping surface. The basic lens design was done with SIMION 7.0 to determine the geometry and electrode voltages of the deceleration lens. The lens consists of eight plates through which the ion beam passes (Fig. 3, top). The first three as well as the last three plates compose two focusing einzel lenses. Plates 1 and 3 are grounded, Plates 6 and 8 are floated at the deceleration potential. Plates 4, 5, and 6 decelerate the ion beam, and are referred to as the deceleration plates. A high voltage power supply and voltage divider provide power to the plates.

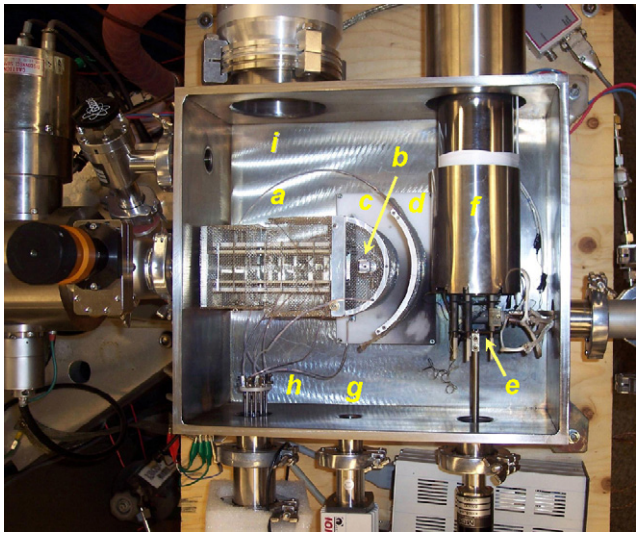

Fig. 2. Top view of the Ping–Pong vacuum chamber and components. (*a*) Deceleration lens assembly; (*b*) Ping plate pivot; (*c*) ion stopping shield; (*d*) electrostatic field shield; (*e*) Pong plate with ion collecting electrostatic lens; (*f*) electrostatic shield for secondary ions; (*g*) vacuum gauge port; (*h*) high voltage feedthroughs for deceleration lens, Ping plate and ion stopper; (*i*) turbomolecular pump port with an ISO100 flange.

The simulations require a precise characterization of the ion beam as it exits the JEOL instrument and enters the deceleration lens. Some important beam characteristics include beam geometry and size at entrance to deceleration lens, divergence angle after the JEOL detector, charge density, and kinetic energy. The JEOL beam shape is a tall, narrow rectangle of a 5-mm height which is essentially constant throughout the JEOL instrument, as determined by the height of the ion source exit slit and collimation by passage through the intermediate (β) and mass resolving (γ) slits. The beam width varies depending on location and slit width settings. The γ slit, located immediately before the detector is fully open to 1 mm. The beam width increases with distance traveled away from the γ slit according to the divergence angle.

The beam vertical divergence is given by the velocity ratio in the forward and vertical directions. Considering ion forward velocities on the order of 10^5 m s^{-1} for 5–10 keV ions and the mean thermal velocity of 150 ms^{-1} at 500 K, the expected vertical divergence angle is only 0.085° and will result in ~0.4 mm beam vertical expansion along the 28.5 cm trajectory from the γ slit to the deceleration lens. The ion beam exiting the JEOL ion optics system diverges horizontally as a result of the slit width and focusing imaging by the electrostatic and magnetic sectors. This is expressed by Eq. (3) [35] which gives beam divergence, β, after passing the γ slit. The variable W_α is the width in mm of the α slit between the ion source and the electrostatic sector. Eq. (3) gives the divergence angle of the ion beam as 0.0107 radians or 0.613 degrees at 2.2 mm width of the α slit. From the γ slit width (1 mm) and the distance between the γ slit and the first deceleration lens (28.5 cm), one calculates the ion beam entering the deceleration lens to be 1.6 mm wide.

$$\beta = W_\alpha \frac{1.88}{387} \text{ (radian/mm)} \tag{3}$$

According to the Helmholtz–Lagrange law, the ion beam divergence angle increases upon deceleration according to Eq. (4), where β_{in} and β_{out} are the incoming and outgoing divergence angle, and T_{in} and T_{out} are, respectively, the incoming and outgoing ion beam kinetic energies. For instance, a 10 keV beam of a 0.613° divergence is dispersed to 19.4° upon deceleration to 10 eV. Thus, refocusing is necessary to obtain near paraxial beam impinging on the Ping

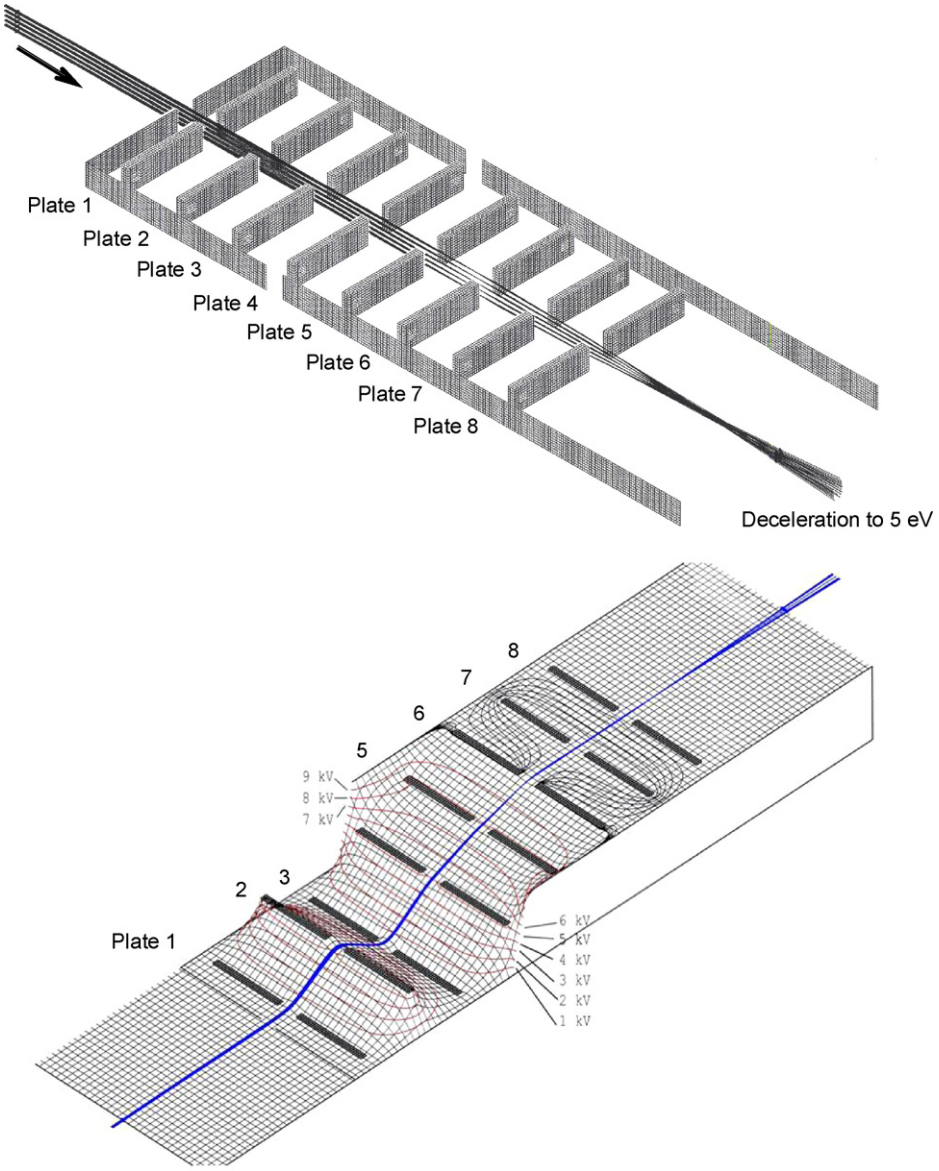

Fig. 3. SIMION potential array and ion trajectories in the deceleration lens. Arrows indicate where the 10 keV ion beam enters the lens. Top: beam of rectangular profile (6.2:1 aspect ratio) after deceleration from 10 keV to 5 eV. Bottom: three-dimensional plot of potentials applied to the deceleration lens.

plate.

$$\beta_{out} = \beta_{in}\sqrt{\frac{T_{in}}{T_{out}}} \quad (4)$$

SIMION 7.0 simulations of potential arrays and ion trajectories were performed in two phases. The initial simulations demonstrated the general shape and electrostatic potentials to be applied to the lens to work properly. The subsequent simulations utilized material and construction restrictions, such as the thickness of a standard stainless steel plates in order to develop a design that would be conveniently built. The final simulation generated a nearly paraxial beam of 5–50 eV kinetic energy by varying only the deceleration potential and the 2nd inner Einzel lens (Fig. 3, bottom). The completed deceleration lens is built out of 0.05″ (1.27 mm) thick stainless steel plates (Kimball Physics), with square apertures of 1.55″ × 0.25 (39.4 mm × 6.35 mm) The 6.2:1 aspect ratio of the aperture reflects the ratio of the horizontal and vertical beam divergence. The plates are stacked on eight electrically insulating alumina rods with 0.6″ (15.24 mm) alumina spacers between the plates. The deceleration lens is mounted on aluminum stands at its front and back ends. The first stand is electrically grounded and has a small aperture (0.2″ × 0.35″, 5.08 mm × 8.89 mm) through which the ion beam enters the deceleration lens. The small aperture ensures that the high electric potentials inside the lens do not penetrate into the flight tube to affect the beam before it enters the deceleration lens. The second stand is charged to the deceleration potential and has a large aperture (1.475″ × 1.475″, 37.46 mm × 37.46 mm) through which the beam passes unaffected. The lens was built using Kimball Physics components; the mounting frames were designed on AutoCAD and built in-house. The optimized voltages from the first plate to the last are 0, 4650, 0, 5700, 8550, 9945, 9700–9945, and 9945 V for 10 keV precursor ions and proportionately lower for lower precursor ion kinetic energies.

The plates are charged using a Bertan 30 W, 10 kV power supply and a voltage divider built from Caddock MQ resistors with resistance error of 0.1%. The voltage divider has three potentiometers to control the voltages distributed on the deceleration lens. The decel-

eration potential can be set to any value between 0 and 10,000 V from its console and is accurate to 1 V. The voltage divider provides output voltages that are proportional to the master deceleration potential from the power supply. The second potentiometer varies the potential on the 7th plate by 200 V without affecting the voltages of the other plates. This 7th plate is the inner lens of the second Einzel lens and controls the focus of the decelerated ion beam. The second potentiometer varies the resistance of the entire circuit so that the voltage of the 2nd, 4th and 5th plates can be adjusted by 100 V. These plates correspond to the inner lens of the 1st Einzel lens and the 2nd and 3rd deceleration plates, respectively.

3.4. Ping surface neutralization and ion stop

Upon exiting the deceleration lens the decelerated beam enters a Faraday cage which is floated at the deceleration potential. The ion beam travels about 3 cm prior to striking the gold plate of the Ping surface, which is also floated at the deceleration potential. The Ping surface is mounted on an electrically insulated rod attached to a rotation motion feedthrough that allows it to be rotated about the vertical axis. This rotational position of the Ping plate defines the incidence angle at which the ion beam impinges on the surface. As described above, the ion beam is presumed to be largely neutralized and the neutrals are scattered off the surface. The scatter angle is defined as the angle between the incoming ion beam and the outgoing deflected neutrals with the Ping surface as the vertex. The neutrals are expected to fan out from the Ping surface with a distribution that varies with both the incidence angle and the ion kinetic energy at impact. The deflection angle is 180° less the scatter angle. The angular distribution of the neutral species is limited between the specular angle and the Ping surface plane.

Neutral species coming off the Ping surface can have a maximum kinetic energy of the acceleration potential in the JEOL less the deceleration potential in Ping–Pong NRMS. This is referred to as the incidence energy. The outgoing neutralized beam will likely have less translational energy than that of the incoming ion beam because of energy deposition in the Ping surface during the collision. For example, if the ions are accelerated to 9950 eV in the JEOL and then decelerated to 9940 eV prior to collision with the Ping surface, the maximum energy the neutrals can carry off the Ping surface is 10 eV without energy loss. One of the goals of this work was to observe and characterize the behavior of neutrals as they depart the Ping surface at various incidence energies and angles.

Ions that survive the Ping collision without being neutralized are prevented from being detected by an ion reflector (Fig. 2 (c)). The latter is a wire mesh electrode, which is floated at a potential 50 V above the deceleration potential and positioned between the Ping and Pong plates so that ions traveling in this direction upon collision with the Ping surface are reflected. The wire mesh allows 95% of neutrals to pass through unaffected. Another wire mesh (Fig. 2(d)) maintained at the ground potential insulates the HV ion stopper from the down-beam ion optic components.

3.5. Pong surface reionization

The Pong surface is made of 0.05-mm thick rhenium ribbon (Goodfellow). The ribbon surface was activated by oxidation [30–34] at approximately 1000 K in 2×10^{-5} Torr partial pressure of oxygen that was admitted through a leak needle valve into the vacuum chamber. The oxidized layer consisting mainly of Re_20_3 is stable through about 1200 K, at which point the volatile Re_2O_7 species is formed and desorbed from the surface [34]. The Pong surface can be resistively heated to 1000–1300 K by a DC current from a Lambda UP20-20 power supply. The temperature was monitored with a K-type thermocouple which was mounted underneath of the Pong ribbon at the closest possible distance.

The Pong ribbon is mounted in an assembly (Figure S1, Supplementary Information) which in turn is mounted on a linear motion feedthrough (LMFT) with a 4″ (101.6 mm) range of travel and can be moved along a line perpendicular to the ion beam. When the LMFT is fully extended, the Pong surface is nearly in line with the ion beam axis along the 0 degree deflection angle. When fully retracted, the Pong surface lies along the 45-degree deflection angle. Therefore, the Pong surface can be positioned anywhere along the first 45 degrees of the deflection angle range. The particular angle the plate makes with the ion beam axis is referred to as the Pong deflection angle. NRMS signal is expected to maximize when the Pong deflection angle and the modal deflection angle are equal. Because the Pong surface must present a face to the neutral beam throughout the 45-degree range of deflection angles, the Pong piece is turned 45 degrees with respect to the quadrupole mass filter axis. In this fashion, the Pong surface presents a perpendicular face to neutrals with a 45-degree deflection angle, and presents a 45-degree face to the neutrals at glancing or near 0-degree deflection angles. The quadrupole is co-axially aligned with the LMFT, and the Pong surface moves linearly farther from quadrupole and the Ping surface as the Pong deflection angle is increased. The NRMS signal therefore can be expected to roughly scale with the cosine of the Pong deflection angle.

The Pong ribbon is spot-welded to two threaded nickel rods through which 13–19 A of heating current flows. The threaded nickel rods run through a 0.5″ (12.7 mm) D machineable ceramic (Macor) rod and are insulated from the other components mounted on the LMFT. The Macor rod stabilizes the two threaded nickel rods, therefore, the Pong surface against the tension from attached wires as the LMFT is moved. The ions are extracted from the ionizing rhenium surface with an einzel lens and focused into the quadrupole mass filter. The extractor lens accelerates and focuses the ions coming off the Pong surface toward the opening of the quadrupole. The extractor is mounted on the LMFT so that the distance between the ionizing surface and the extractor lens remains constant. The distance between the extractor lens and the quadrupole entrance changes as the LMFT position is changed. SIMION 7.0 was used to design the voltage and geometry of the einzel lens.

3.6. Experimental operation and results of Ping–Pong NRMS

Obtaining a Ping–Pong NR mass spectrum consists of several steps. First, an ion beam is produced in the JEOL ion source and the desired ions are mass selected by the JEOL double focusing ion optics system. The ions can be detected before they enter the Ping–Pong chamber by temporarily turning on the JEOL conversion dynode and electron multiplier voltages. However, both voltages must be turned off to allow the ions to pass to the Ping–Pong chamber. The ions are then decelerated and the ion current reaching the Ping plate is measured. To avoid excessive ion beam divergence after deceleration and also to prevent intermittent problems with HV breaks and arcing, we used 5 keV mass-selected ions from the JEOL instrument. Second, the mass-selected ion current is detected on the Ping surface floated at a potential close to 5000 V and its dependence on the ion kinetic energy and incident angle is determined. Third, hyperthermal neutral species scattered from the Ping plate are allowed to strike the Pong surface and get reionized. Since this step involves adjusting several parameters, such as the Pong plate position, temperature, and surface treatment, it turned out to be the most difficult and least controllable one. Last, the extractor lens voltages must be tuned to refocus the reionized particles into the quadrupole mass filter for mass analysis and detection. These individual steps will be addressed in the following paragraphs. Most

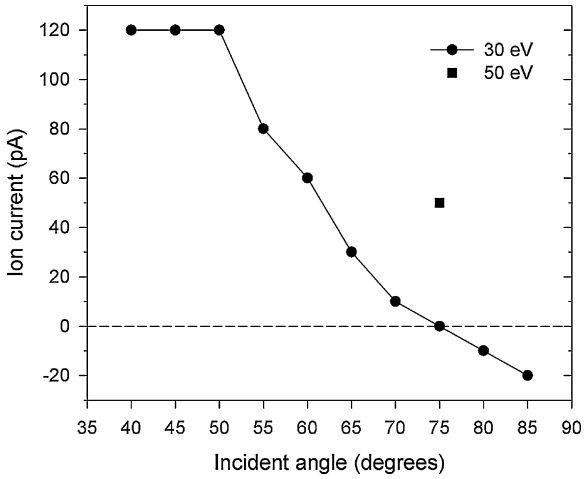

Fig. 4. Incident angle dependence of the ion current at the Ping plate. Mass selected *m/z* 79 ions from pyridine at an initial kinetic energy of 5 keV after deceleration to 30 and 50 eV.

measurements were carried out with stable molecular ions of pyridine and benzene whose properties in surface collisions haven been studied thoroughly under a variety of conditions [36,37].

3.7. Ion current detection on the Ping plate

A beam of $C_5H_5N^{+\bullet}$ ions from 70-eV electron ionization of pyridine was accelerated to 5 keV, mass selected, and positioned on the γ-slit of the JEOL instrument. The JEOL magnet sector was held stationary to pass the *m/z* 79 ions and the ion current of $C_5H_5N^+$ remained stable during the operation. For $C_5H_5N^{+\bullet}$ surface ion current measurements, the Ping plate was turned perpendicular to the ion beam (0° incident angle) and connected to a picoammeter that was floated at the deceleration potential. In the absence of the ion beam, the background current collected at the plate and connecting cables floated at 5 kV was <30 pA. A plot of the ion current of decelerated $C_5H_5N^{+\bullet}$ versus the deceleration potential is shown in Figure S2, Supplementary Information. The ion current at the Ping plate is steady at 70 pA up to 5040 V and then it falls to zero at 5050 V. The retarding potential at which the ion current fell to one half of its mean value (5045 V) was used to calibrate the precursor ion kinetic energy. Note that the JEOL acceleration potential is adjusted by a multi-turn potentiometer that can be changed in ca. 50 V steps. The kinetic energy of the ions impinging on the Ping plate is determined by the difference between the potential applied on the last element of the deceleration lens and the stopping potential.

The effect on the collected ion current of the incident angle were measured at 30 and 50 eV nominal collision energy. Note that as the Ping plate is rotated from the 0° incident angle the beam-surface cross-section changes. The dependence of the collected current of $C_5H_5N^+$ on the incident angle, after correction for the angle-independent background current, is shown in Fig. 4. The current measured for 30 eV ions was constant up to ca. 50° incident angle and then it decreased to zero at 75°. At more glancing angles the measurements showed small negative currents which could be due to secondary electrons from ions hitting the lens or shield elements.

The 50 eV beam gave a positive ion current of 50 pA even at 75° incident angle. Therefore, 50 eV kinetic energy and incident angles between 60 and 75° were used in all subsequent measurements.

Ion neutralization is presumed to proceed by electron transfer (ET) from the Ping surface to the impinging precursor ion. The ET efficiency depends on the ion beam incident angle, precursor ion recombination energy, and surface material work function. We tested gold, copper and aluminum Ping surfaces whose properties are summarized in Table 1. Best results were obtained with vapor-depositing a 150–200 nm gold layer on a highly polished aluminum substrate (30 mm × 25 mm × 1 mm), which gave flat and conductive Ping plates that were easy to mount and conductively connect to the power supply and picoammeter. Vapor-deposited gold on glass or quartz also gave flat surfaces, but those were more difficult to connect. Solid gold foils (Goodfellow, 99.99%) were difficult to keep flat, while copper and aluminum surfaces underwent oxidation in the vacuum chamber upon exposure to oxygen.

Recombination energies of the precursor ions used for surface neutralization were found to have an effect on the ion currents measured on the Ping plate. Table 2 shows that precursor ions with higher recombination energies gave higher neutralization currents on vapor deposited gold surfaces. This was despite the fact that the work function of gold (5.1 eV) was lower than the recombination energies of the precursor ions used here, and thus electron transfer was exoergic. The dependence of ion recombination energy indicates that charge transfer with the surface was kinetically controlled and ions of lower recombination energies were sputtered off the surface before they undergo charge exchange neutralization.

Table 2
Neutralization current for precursor ions of different recombination energies striking gold surface at 50 eV

Ion	Recombination energy (eV)	Ion current (pA)	Incident angle
Pyridine$^{+\bullet}$	9.26	~120	60
Benzene$^{+\bullet}$	9.24	~120	60
Furan$^{+\bullet}$	8.8	<70	60
Aniline$^{+\bullet}$	7.7	<20	60

3.8. Ping–Pong NRMS of pyridine

Based on the neutralization current and ionization energy, pyridine was chosen as a test compound for the Ping–Pong experiments. To obtain a Ping–Pong neutralization-reionization mass spectrum, mass-selected *m/z* 79 ions were produced by the JEOL mass spectrometer, decelerated to 49 eV, and allowed to collide with a gold Ping surface at 75 degree incident angle. The Pong plate (Re ribbon) was activated with oxygen 2×10^{-5} Torr with oxygen and heated to 1003 ± 5 K. The Pong plate was positioned to collect neutrals coming off the Ping plate at 5° to its surface. The reionized ion current disappeared when the Pong plate was moved ~5 mm away or

Table 1
Properties of Ping plate surface materials

Material	Work function (eV)	Drawbacks	Advantages
Gold foil (99.99%)	5.1	Rough surface	Stable and pure
Copper (0.5 mm)	4.7	Easily oxidized	Low work function
Aluminum (0.5 mm)	4.08	Easily oxidized	
Gold film (200 nm)/glass (0.3 mm)	5.1	Difficult to mount and low conductance	Smooth surface
Gold film (200 nm)/quartz (0.3 mm)	5.1		
Gold film (200 nm)/aluminum (1 mm)	5.1	Thin film	Smoother than gold foil, inexpensive

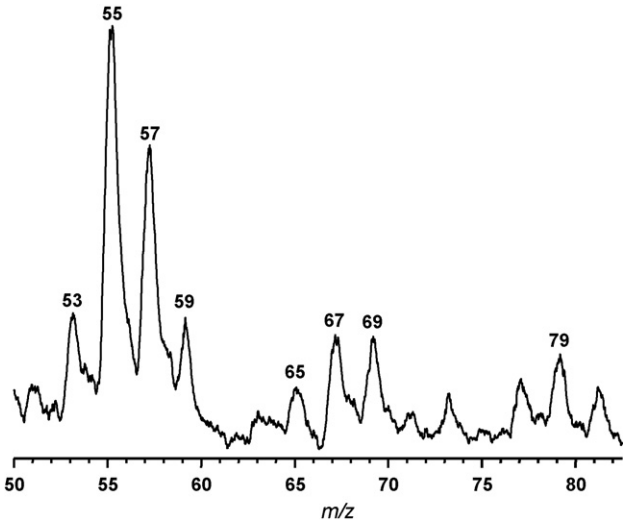

Fig. 5. Surface neutralization (Au)/surface reionization (Re) spectrum of the *m/z* 79 ion from pyridine. The precursor ion translational energy was 49 eV, the incident angle was 75 degrees. The deflection angle was ~5 degrees to the Ping surface. The Ping plate was a gold foil, the Pong plate was an oxygen-activated Re ribbon.

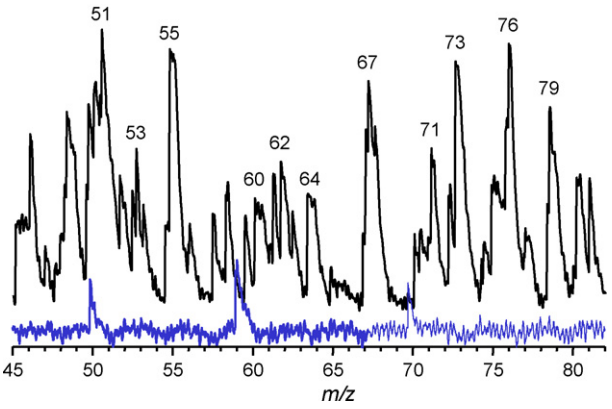

Fig. 6. Surface neutralization/surface reionization (Re) spectrum of the *m/z* 78 ion from benzene. The translational energy was 18 eV, the incident angle was 70 degrees. The deflection angle was ~16 degrees to the Ping surface. The Ping plate was a gold foil, the Pong plate was an oxygen-activated Re ribbon at 1110 K. The blue trace shows the background reionization signal in the absence of precursor benzene ions.

towards the quadrupole mass filter. This indicated that hyperthermal neutral species were coming off the Ping plate in a relatively narrow angle (4°) following exposure to the 49 eV pyridine ion beam.

The Ping–Pong NR mass spectrum of pyridine obtained by neutralization on a gold surface is shown in Fig. 5. The spectrum was scanned from *m/z* 50 up to avoid the abundant peaks of Na^+ and K^+ corresponding to ions thermally desorbed from the Pong Macor material. We note that the desorbed Na^+ and K^+ ions were detected at practically any position of the Pong plate, which indicated that the electrostatic extraction lens collected ions coming off the Pong surface and focused it into the quadrupole mass filter. The spectrum shows a peak at *m/z* 79 that may correspond to reionized pyridine. However, the spectrum also shows numerous peaks (*m/z* 81, 73, 69, 67, etc.) that cannot be assigned to the pyridine ion or its ion or neutral dissociation products. Previous studies of surface-induced dissociation of pyridine ions showed the most abundant fragments to be at *m/z* 78, 53, 52, and 39. Although these ions are present in the Ping–Pong NR mass spectrum in Fig. 5, they are much less abundant than the peaks that do not originate from pyridine dissociations. Pyridine is known to pick up a hydrogen atom from surface adsorbates to give an $(M+H)^+$ ion at *m/z* 80 [36a–d]. Although the corresponding (pyridine + H) radical is stable [38], the peak of *m/z* 80 is practically absent in the Ping–Pong NR mass spectrum (Fig. 5).

Ping plates made of aluminum and copper were also tried as surfaces for neutralization of pyridine ions. For the aluminum plate, 57 eV pyridine ions were collided at 75 degree incident angle and the outgoing neutrals were reionized at an angle close to 0 degrees to the Ping plate surface. The Pong plate was an Re ribbon at 1019 ± 6 K. For the copper Ping plate, 45 eV pyridine ions were collided at 70 degree incident angle, neutrals were collected at a 6–7 degree angle to the plate surface and reionized on the Pong plate at 1042 ± 6 K. However, the Ping–Pong NR mass spectra from these surfaces were of an even worse quality than those from the gold surface despite the finding that the neutralization currents on the aluminum and copper surfaces were higher than that on the gold surface. Although copper and aluminum have lower work functions than gold, their surfaces are easily oxidized and this surface modification presumably affects the neutrals sputtered off the surface.

3.9. Ping–Pong NRMS of benzene

Benzene has a similar ionization energy as pyridine but the benzene ion undergoes less extensive pick-up reactions upon collisions with surfaces [37]. We attempted to obtain a Ping–Pong NR mass spectrum of benzene. Mass-selected *m/z* 78 benzene ions were collided at 18 eV on a gold-coated (150 nm) aluminum plate at a 70-degree incident angle and the sputtered neutrals were reionized on the Pong plate positioned at 16 degrees off the Ping plane and heated to 1110 K. The spectrum (Fig. 6) shows mostly hydrocarbon ions, some of which can be assigned to benzene fragments, e.g., *m/z* 77, 52, and 51 [37a]. However, most of the peaks in the spectrum do not originate from unimolecular dissociations of benzene and must be due to hyperthermal neutrals sputtered from the Ping surface.

4. Discussion

The above-described experiments indicate that neutralization of hyperthermal organic ions on metal surfaces is not a simple process that would abundantly yield intact molecules. Under our conditions, the gold surface is covered by an adsorbate, most likely hydrocarbons deposited from the residual gas phase at 10^{-7}–10^{-6} Torr [36a]. However, the adsorbed molecules should not prevent 40–50 eV incident ions from reaching the metal surface and undergo neutralization [36c]. The ion current measurements indicate that ion discharge does occur on the Ping plate. The rather sharp angular dependence of the NRMS signal also indicates that the species being reionized on the Pong plate leave the Ping plate at non-specular angles. Due to the Langmuir–Saha equation (Eq. (1)), only molecules with hyperthermal kinetic energies are efficiently ionized on the Re surface. The current results can be tentatively interpreted by the following model. Impact on the Ping plate of hyperthermal precursor ions results in their neutralization and simultaneous sputtering of molecules adsorbed on the surface. A fraction of the sputtered molecules have hyperthermal kinetic energies and reach the Pong plate together with a fraction of the neutralized precursor species to be reionized. The fact that mainly even-electron hydrocarbon ions are detected in the Ping–Pong NR mass spectra can be due to the low ionization energies of hydrocarbon radicals formed on the Ping plate for which high surface ionization efficiencies can be expected. Alternatively, dissociations of hydrocarbon ions that were formed on the Pong plate can take place before mass analysis, as observed in surface-induced disso-

ciation [36a]. Our current experimental set up does not allow us to distinguish these processes.

5. Conclusions

Collisional neutralization of hyperthermal organic ions on gold surfaces does not yield abundant flux of hyperthermal neutral molecules. Rather, collisional reionization indicates that most of the neutral species coming off the surface are due to sputtered adsorbate. Further modifications of the Ping and Pong plate material and instrument design will be necessary to make Ping–Pong NR mass spectrometry a practically usable method.

Acknowledgments

Support for this research was provided by the National Science Foundation (Grant CHE-0349595) and the University of Washington Royalty Research Fund.

Appendix A. Supplementary data

Supplementary data associated with this article can be found, in the online version, at doi:10.1016/j.ijms.2008.07.022.

References

[1] B.W. Williams, R.F. Porter, J. Chem. Phys. 73 (1980) 5598.
[2] P.C. Burgers, J.L. Holmes, A.A. Mommers, J.K. Terlouw, Chem. Phys. Lett. 102 (1983) 1.
[3] P.O. Danis, C. Wesdemiotis, F.W. McLafferty, J. Am. Chem. Soc. 105 (1983) 7454.
[4] (a) C. Wesdemiotis, F.W. McLafferty, Chem. Rev. 87 (1987) 485;
(b) J.K. Terlouw, H. Schwarz, Angew. Chem. 99 (1987) 829;
(c) J.L. Holmes, Mass Spectrom. Rev. 8 (1989) 513;
(d) J.K. Terlouw, Adv. Mass Spectrom. 11B (1989) 984;
(e) F. Tureček, Org. Mass Spectrom. 27 (1992) 1087;
(f) D.V. Zagorevski, J.L. Holmes, Mass Spectrom. Rev. 13 (1994) 133;
(g) N. Goldberg, H. Schwarz, H. Acc. Chem. Res. 27 (1994) 347;
(h) C.A. Schalley, G. Hornung, D. Schröder, H. Schwarz, Chem. Soc. Rev. 27 (1998) 91;
(i) D.V. Zagorevski, J.L. Holmes, Mass Spectrom. Rev 18 (1999) 87;
(j) F. Tureček, Top. Curr. Chem. 225 (2003) 77;
(k) F. Tureček, in: P.B. Armentrout (Ed.), Encyclopedia of Mass Spectrometry, vol. 1, Elsevier, Amsterdam, 2003, p. 528 (Chapter 8).
[5] F. Tureček, M. Gu, S.A. Shaffer, J. Am. Soc. Mass Spectrom. 3 (1992) 493.
[6] (a) D.W. Kuhns, S.A. Shaffer, T.B. Tran, F. Tureček, J. Phys. Chem. 98 (1994) 4845;
(b) D.W. Kuhns, F. Tureček, Org. Mass Spectrom. 29 (1994) 463.
[7] C.A. Schalley, G. Hornung, D. Schroder, H. Schwarz, Int. J. Mass Spectrom. Ion Process. 172 (1998) 181.
[8] M. Sadílek, F. Tureček, J. Phys. Chem. 100 (1996) 9610.
[9] (a) M. Sadílek, F. Tureček, Chem. Phys. Lett. 263 (1996) 203;
(b) V.Q. Nguyen, M. Sadílek, A.J. Frank, J.G. Ferrier, F. Tureček, J. Phys. Chem. A 101 (1997) 3789;
(c) A.J. Frank, M. Sadílek, J.G. Ferrier, F. Tureček, J. Am. Chem. Soc. 119 (1997) 12343;
(d) A.J. Frank, F. Tureček, J. Phys. Chem. A 103 (1999) 5348;
(e) M. Polášek, F. Tureček, J. Phys. Chem. A 105 (2001) 1371.
[10] (a) O.V. Boltalina, P. Hvelplund, T.J.D. Jørgensen, M.C. Larsen, M.O. Larsson, D.A. Sharoitchenko, M. Sørensen, Phys. Rev. A 62 (2000) 023202;
(b) M.O. Larsson, P. Hvelplund, M.C. Larsen, H. Shen, H. Cederquist, H.T. Schmidt, Int. J. Mass Spectrom. 177 (1998) 51.
[11] (a) G.C. Shields, P.A. Steiner IV, P.R. Nelson, M.C. Trauner, T.F. Moran, Org. Mass Spectrom. 22 (1987) 64;
(b) J.B. Sedgwick, P.R. Nelson, P.A. Steiner IV, T.F. Moran, Org. Mass Spectrom. 23 (1988) 256;
(c) J.B. Sedgwick, P.R. Nelson, C.A. Jordan, L.E. Abbey, Y. Xu, T.F. Moran, Chem Phys. Lett. 146 (1988) 113;
(d) J.R. Regalado, W.M. Holbrook, D.E. Bostwick, T.F. Moran, Org. Mass Spectrom. 25 (1990) 174;
(e) M.-Y. Zhang, F.W. McLafferty, J. Am. Soc. Mass Spectrom. 3 (1992) 108.
[12] C.E.C.A. Hop, J.L. Holmes, Org. Mass Spectrom. 26 (1991) 476.
[13] (a) C.E.C.A. Hop, J.L. Holmes, Int. J. Mass Spectrom. Ion Process. 104 (1991) 213;
(b) V.Q. Nguyen, F. Tureček, J. Mass Spectrom. 31 (1996) 843.
[14] F. Tureček, M. Gu, C.E.C.A. Hop, J. Phys. Chem. 99 (1995) 2278.
[15] E.A. Syrstad, S. Vivekananda, F. Tureček, J. Phys. Chem. A 105 (2001) 8339.
[16] J.K. Wolken, F. Tureček, J. Phys. Chem. A 105 (2001) 8352.
[17] J.W. Rabalais (Ed.), Low Energy Ion–Surface Interactions, Wiley, Chichester, 1994.
[18] R.G. Cooks, T. Ast, T. Pradeep, Acc. Chem. Res. 27 (1994) 316.
[19] V. Grill, J. Shen, C. Evans, R.G. Cooks, Rev. Sci. Instr. 72 (2001) 3149.
[20] A.L. McCormack, J.L. Jones, V.H. Wysocki, J. Am. Soc. Mass Spectrom. 3 (1992) 859.
[21] L. Hanley, O. Kornienko, E.T. Ada, E. Fuoco, J.L. Trevor, J. Mass Spectrom. 34 (1999) 705.
[22] J. Laskin, T.H. Bailey, J.H. Futrell, J. Am. Chem. Soc. 125 (2003) 1625.
[23] J. Žabka, Z. Dolejšek, J. Roithová, V. Grill, T.D. Märk, Z. Herman, Int. J. Mass Spectrom. 213 (2002) 145.
[24] B.H. Cooper, E.R. Behringer, in: J.W. Rabalais (Ed.), Low Energy Ion–Surface Interactions, Wiley, Chichester, 1994, p. 264, Chapter 5.
[25] E.B. Dahl, E.R. Behringer, D.R. Andersson, B.H. Cooper, Int. J. Mass Spectrom. Ion Process. 174 (1998) 267.
[26] L. Hanley, H. Lim, D.G. Schultz, S. Garbis, C. Yu, E.T. Ada, M.B.J. Wijesundara, Nucl. Instr. Methods Phys. Res. B 157 (1999) 174.
[27] H.F. Winters, H. Coufal, C.T. Rettner, D.S. Bethune, Phys Rev. B 41 (1990) 6240.
[28] S.B. Wainhaus, H. Lim, D.G. Schultz, L. Hanley, J. Chem. Phys. 106 (1997) 10329.
[29] H. Kishi, T. Fujii, J. Chem. Phys. 108 (1998) 1940.
[30] H. Kishi, T. Fujii, Int. J. Mass Spectrom. 194 (2001) 75.
[31] T. Fujii, Y. Inagaki, Y. Mitsutsuka, Int. J. Mass Spectrom. Ion Process. 124 (1991) 45.
[32] A. Amirav, Org. Mass Spectrom. 26 (1991) 1.
[33] A. Danon, A. Amirav, Int. J. Mass Spectrom. Ion Process. 125 (1993) 63.
[34] S. Danon, A. Amirav, J. Am. Soc. Mass Spectrom. 4 (1993) 869.
[35] Formula 3 was kindly provided by JEOL, Inc.
[36] (a) T. Ast, M.A. Mabud, R.G. Cooks, Int. J. Mass Spectrom. Ion Process. 82 (1988) 131;
(b) T.E. Kane, A. Somogyi, V.H. Wysocki, Org. Mass Spectrom. 28 (1993) 1665;
(c) Q. Wu, L. Hanley, J. Phys. Chem. 97 (1993) 2677;
(d) S.B. Wainhaus, J.A. Burroughs, L. Hanley, Surf. Sci. 344 (1995) 122;
(e) L.M. Phelan, M.J. Hayward, J.C. Flynn, S.L. Bernasek, J. Phys. Chem. B 102 (1998) 5667.
[37] (a) V.H. Wysocki, J.-M. Ding, J.L. Jones, J.H. Callahan, F.L. King, J. Am. Soc. Mass Spectrom. 3 (1992) 27;
(b) K. Vékey, A. Somogyi, V.H. Wysocki, J. Mass Spectrom. 30 (1995) 212;
(c) M.J. Hayward, F.D.S. Park, L.M. Manzella, S.L. Bernasek, Int. J. Mass Spectrom Ion Process. 148 (1995) 25;
(d) W. Zhong, E.N. Nikolaev, J.H. Futrell, V.H. Wysocki, Anal. Chem. 69 (1997) 2496;
(e) R. Worgotter, J. Kubišta, J. Žabka, Z. Dolejšek, T.D. Märk, Z. Herman, Int. J. Mass Spectrom. Ion Process. 174 (1998) 53.
[38] V.Q. Nguyen, F. Tureček, J. Mass Spectrom. 32 (1997) 55.